J Electroceram (2009) 22:24–32
DOI 10.1007/s10832-008-9432-3

Electrical conductivity of ceria nanoparticles under high pressure

H. Takamura · J. Kobayashi · N. Takahashi · M. Okada

Received: 14 March 2007 / Accepted: 21 January 2008 / Published online: 13 February 2008

Abstract This paper describes the electrical conductivity of ceria nanoparticles under high pressure ranging from 2 to 6 GPa. The samples used were pure and acceptor-doped ceria nanoparticles with a grain size of approximately 2 nm prepared by mixing hexamethylenetramine and metal nitrate solutions. The size of ceria nanoparticles was controlled to be 2 to 15 nm by varying heat-treatment conditions. The in-situ electrical conductivity measurements under high pressure were conducted by using an ac-impedance spectroscopy. By applying a pressure of 6 GPa at 300 °C, the green compact of 6 mol % Sm-doped ceria nanoparticles was densified; a relative density of 93% was achieved. The sample showed an electrical conductivity of 3×10^{-3} S/cm at 300 °C under 6 GPa. The enhancement of electrical conductivity under high pressure seems to be related to ionic conduction in the vicinity of grain boundaries.

Keywords Sm-doped ceria · Ion conductivity · Grain boundary · Ac impedance

1 Introduction

Pure and accepter-doped cerium dioxides have been widely investigated because of their variety of electrical conductivity and high catalytic activity. For example, Sm-doped ceria is used as an electrolyte in low-temperature solid oxide fuel cells (LT-SOFCs). On the other hand, Pr- and Mn-doped ceria can be applied to oxygen permeable ceramics and to an anode electrode in the SOFCs because of their high mixed ionic and electronic conductivity [1–4]. To enhance their functionalities, ceria nanoparticles have been attracting much attentions of many researchers. To date, a large number of papers have been published with respect to the electrical transport properties of ceria nanoparticles. Chiang et al. reported the enhancement of n-type electronic conductivity by four orders of magnitude for dense ceria nanoparticles with an average grain size of 10 nm [5, 6]. This behavior has been also observed for acceptor-doped ceria with different doping levels, and explained in conjunction with the presence of a space charge layer which causes the exponential increase in electronic carrier concentration, and simultaneously, the suppression of oxygen vacancy concentration in the vicinity of the interfacial layer [7–13].

In this paper, to clarify the nature of oxide-ion conductivity of ceria nanoparticles, the authors prepared acceptor-doped ceria nanoparticles, and conducted the *in-situ* ac-impedance measurements under high pressure on the order of giga pascal. The use of high pressure enables one to prevent nanoparticles from grain growth, and as a result, to obtain dense sample at lower temperatures. Moreover, such high pressure seems to affect the structure of grain boundary regions, in other words, modify the effects of space charge layer on charged carriers. The purpose of this study is to prepare the accepter-doped ceria nanoparticles, where the acceptor is Sm, Pr, and Mn, and then to clarify the electrical conductivity of the ceria nanoparticles under high pressure.

H. Takamura (✉) · J. Kobayashi · N. Takahashi · M. Okada
Department of Materials Science, Tohoku University,
6-6-11-301-2 Aramaki Aza Aoba, Sendai 980-8579, Japan
e-mail: takamura@material.tohoku.ac.jp

2 Experimental details

Sm, Pr and Mn-doped ceria nanoparticles have been prepared by mixing nitrate solutions and hexamethylenetetramine (HMTA) as an oxidizing agent [14, 15]. The mixed solution was stirred at room temperature. To control pH of solutions, hydrogen peroxide solution (30–35.5 vol% H_2O_2) was added. The mixed solution was centrifuged to obtain precipitates. The resultant powders were washed with distilled water for four times to eliminate the residual reagents. The powders were then rinsed with isopropyl alcohol, and dried at 100 °C in air. Furthermore, to evaluate grain growth behavior, the dried powders were calcined for 10 h at various temperatures ranging from 100 to 700 °C. Phase identification was performed by means of powder X-ray diffractometry. As a reference sample, a bulk sample of Sm-doped ceria was prepared by the Pechini process followed by sintering at 1500 °C for 20 h. The resultant sintered body was found to show a relative density of approximately 93% and a grain size of approximately 2 to 5 μm.

Average particle size of the oxide powders was estimated by an X-ray line broadening technique performed on the diffraction peaks of ceria phases. The intrinsic profile broadening (β) can be given by $\beta = \beta_{\exp} - \frac{\beta_{\text{ins}}^2}{\beta_{\exp}}$, where $\beta_{\exp}$ is the experimentally observed profile broadening, β_{ins} the convolution of the profile broadening due to instruments. Klug and Alexander have reported that this approximation well represents the intrinsic broadening [16]. Furthermore, suppose that the grain size and micro-strain broadening were described by using Cauchy–Gaussian (CG) relationship, He et al. and Zang et al. reported that the CG approximation is the most appropriate method for the linear fitting for grain size and micro-strain [17, 18]; the following equation can be derived:

$$\frac{\beta^2}{\tan^2\theta} = \frac{K\lambda}{D}\frac{\beta}{\tan\theta\sin\theta} + 16e \tag{1}$$

where $K = 0.9$, λ is the wave length of CuK_α ($\lambda = 0.15418$ nm), θ is a diffraction angle, e is an approximate upper limit of the lattice distortion [16] and D is a grain size. When $\frac{\beta^2}{\tan^2\theta}$ is plotted as a function of $\frac{\beta}{\tan\theta\sin\theta}$, the slope should be $\frac{K\lambda}{D}$.

The specific surface area of nano-sized ceria was determined by BET analysis based on the results of nitrogen adsorption at 77 K. From the BET surface area, particle size can be also estimated by the following equation:

$$D = \frac{6\times 10^3}{d\cdot S} \tag{2}$$

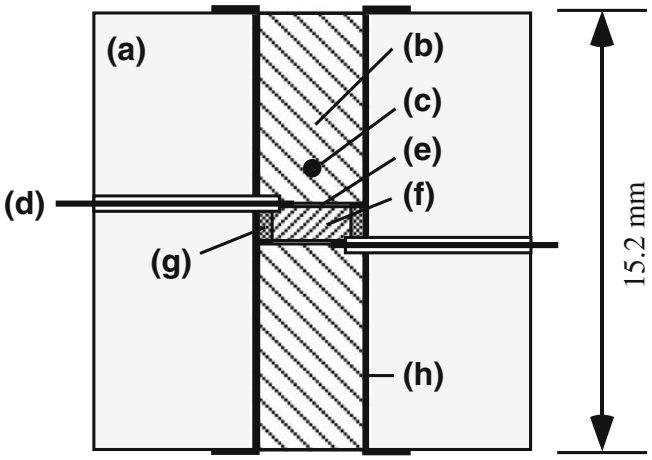

Fig. 1 Schematic diagram of measurement cell with: (a) pressure transmitting media (pyrophyllite), (b) boron nitride rod, (c) thermocouple (chromel-alumel), (d) Pt lead wire, (e) Pt-gauze current collector, (f) sample, (g) boron nitride ring, and (h) nichrome heater tube

where D is the average particle size, S is the specific surface area, d is the theoretical density.

High pressure conductivity measurements were conducted by using a cubic anvil-type apparatus, which enables to give pseudo isostatic pressure in the range of 2 to 6 GPa [19]. Prior to conductivity measurements, pressure as a function of load applied was calibrated by pressure-induced transformation points of Bi (2.55 and 2.7 GPa), Tl (3.7 GPa) and Ba (5.5 GPa). Figure 1 shows a schematic diagram of conductivity measurement cell. All components including a thermocouple (K-type), Pt gauzes, and lead wires were precisely built in a cubic-shape pyrophyllite cell which work as pressure-transmitting media. The electrical conductivity was obtained by means of complex impedance analysis in the frequency range of 0.01 Hz to 10 MHz.

3 Results and discussion

3.1 Synthesis and size characterization

The acceptor-doped ceria nanoparticles were prepared with 200 μL/dL H_2O_2 addition and stirring for 1 h. The oxidizing agent, HMTA, has a unique characteristic of hydrolyzing quite slowly to produce formaldehyde under acidic circumstances [20].

$$C_6H_{12}N_4 + 6H_2O = 6H_2CO + 4NH_3 \longrightarrow NH_3 + H_2O = NH_4OH \tag{3}$$

When the pH value was low, the hydrolysis was favored, which led to the large critical supersaturation for nucleation of the precipitates. Because of this, H_2O_2 added samples showed relatively large yields. The detailed reaction process and the effect of the addition of H_2O_2 were described elsewhere [21]. As a result, the Sm-, Pr-, and Mn-doped ceria nanoparticles with particle size of 2-3 nm were successfully prepared. Even though the nominal composition of the doped ceria was $Ce_{0.6}Sm_{0.4}O_{2-\delta}$, $Ce_{0.5}Pr_{0.5}O_{2-\delta}$, and $Ce_{0.5}Mn_{0.5}O_{2-\delta}$, the actual one was found to be $Ce_{0.94}Sm_{0.06}O_{2-\delta}$, $Ce_{0.95}Pr_{0.05}O_{2-\delta}$, and $Ce_{0.92}Mn_{0.08}O_{2-\delta}$, respectively.

Figure 2 shows XRD patterns of Sm-doped ceria nanoparticles annealed at various temperatures. All the samples were identified to have a fluorite structure. As a reference, a bulk sample with a grain size larger than 1 μm is also shown in Fig. 2, which is used to determine the profile broadening due to instrument optics. After annealing, the shape of reflections tends to be sharp. The particle size obtained from the line-broadening analysis and BET surface area as a function of annealing temperature was plotted in Fig. 3. The particle size increases with increasing annealing temperature. At 100 °C, the particle size of pure and the acceptor-doped ceria nanoparticles determined from XRD was approximately 3 nm. Even after annealing at 600 °C for 10 h, the size of less than 15 nm was kept. The particle size calculated from BET analysis gives a slightly larger grain size than that calculated from XRD. At 100 °C, the particle size calculated from BET

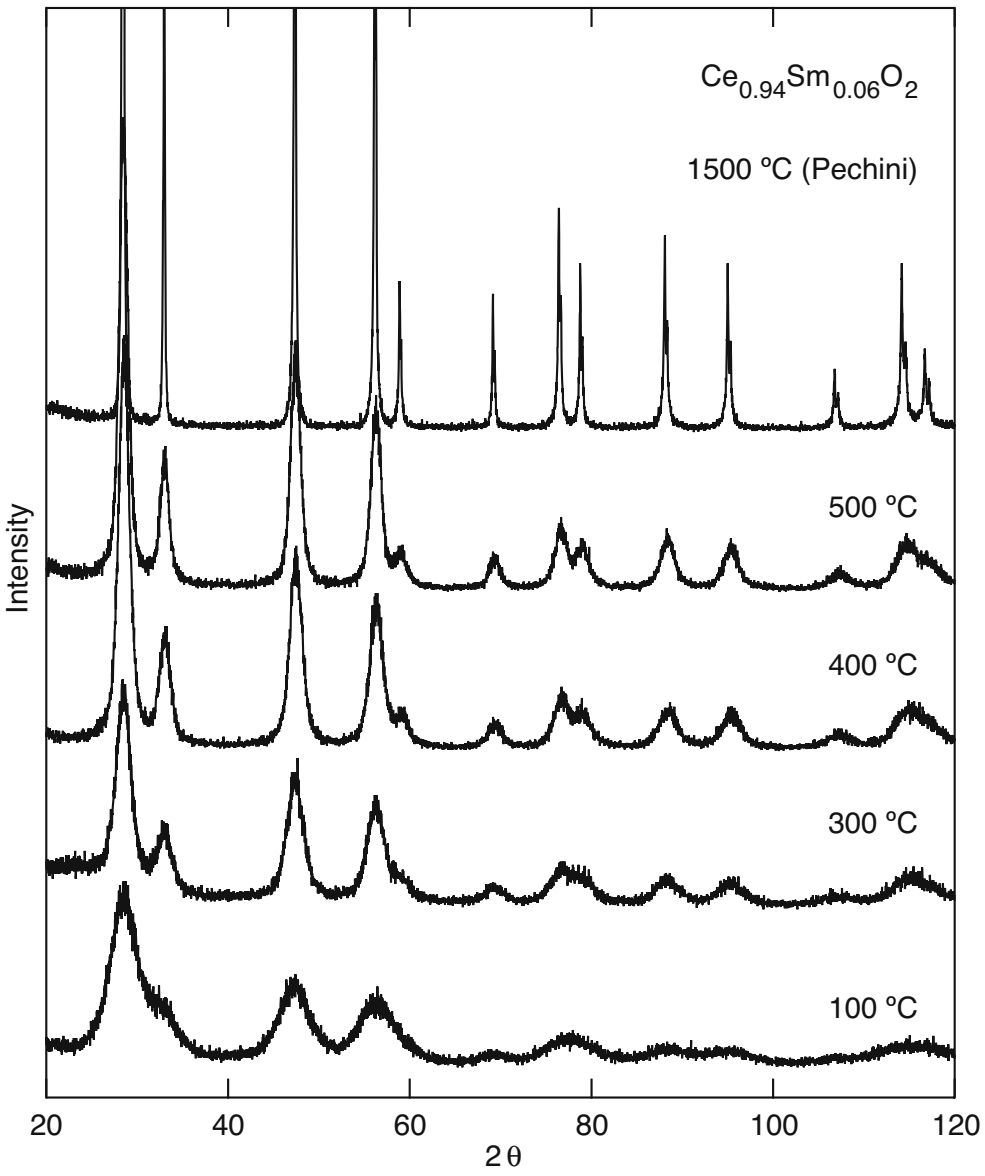

Fig. 2 X-ray diffraction patterns of 6 mol%Sm-doped ceria nanoparticles annealed at T °C for 10 h (T = 100 – 500), and 5 mol%Sm-doped ceria prepared by the Pechini process and sintering at 1500 °C (top)

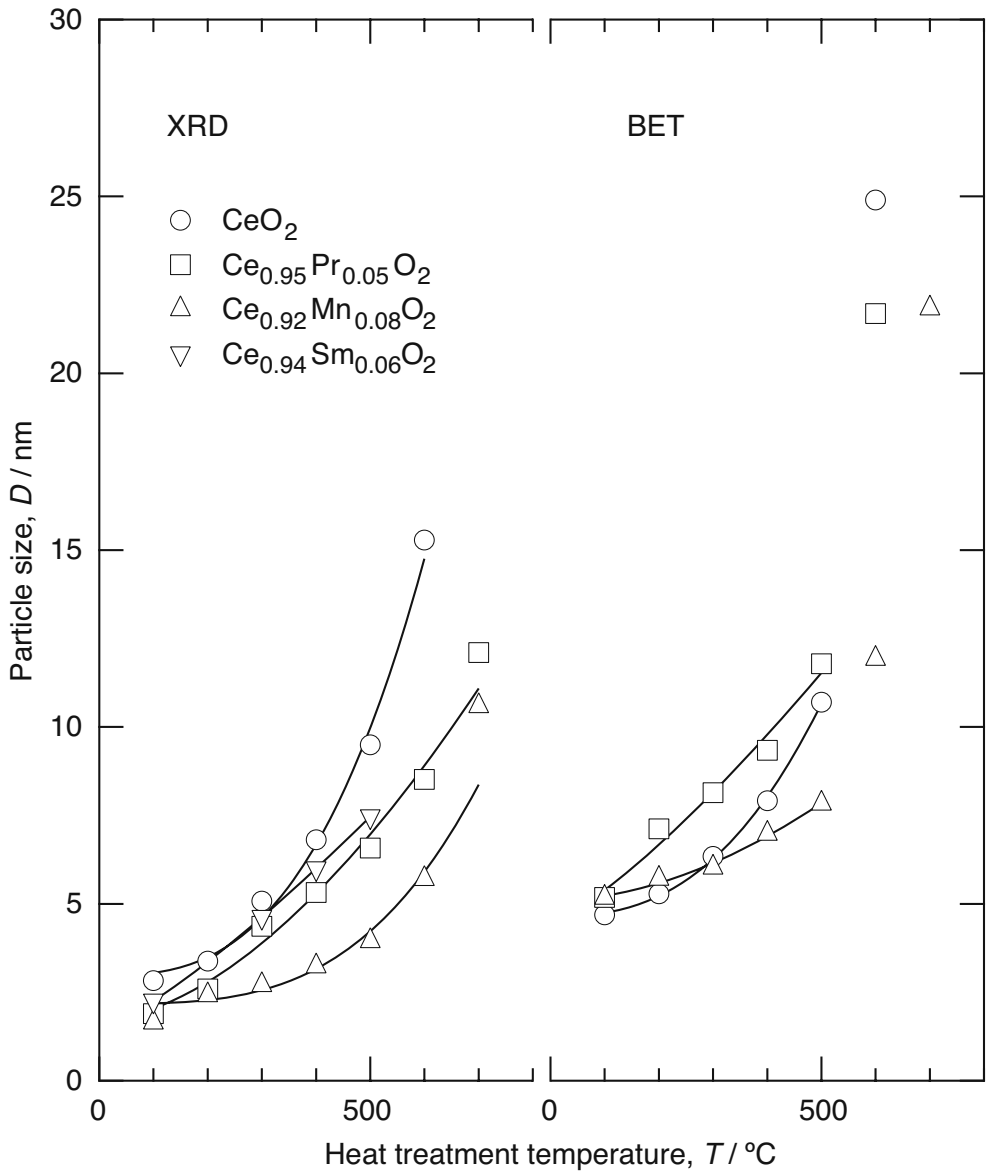

Fig. 3 Heat-treatment temperature dependence of particle size determined from XRD and BET methods

was approximately 5 nm. This difference in particle sizes suggests that the nanoparticles form agglomerates. To clarify this point, the pore size distribution of the ceria nanoparticles annealed at 100 °C and 600 °C for 10 h were performed. Based on the shape of the adsorption isotherms, all samples in this study were characterized as a type IV with a hysteresis loop at intermediate relative pressures. Pore size distribution was calculated by means of DH (Dollimore-Heal) plot. The Pr-doped ceria showed a narrow pore volume distribution. In contrast, the Mn-doped ceria had a wide distribution and the pore size was approximately 5 nm. This pore size seems to correspond to a space between nanoparticles in the agglomerates. In this study, the size of ceria nanoparticles were controlled by adjusting the annealing temperature.

Figure 4 shows the lattice constant of the ceria nanoparticles as a function of particle size. In the figure, the valence of Ce predicted by Tsunekawa et al. [22] is also plotted. The lattice constant increases with decreasing the particle size. At 600 °C, the lattice constant of pure and acceptor-doped ceria nanoparticles was approximately 0.5411 nm, which was almost comparable to that of bulk state (0.5410 nm). This change in the lattice constant shows a good agreement with the valence change of Ce cations predicted by Tsunekawa et al. To explain lattice expansion behavior in ceria nanoparticles, they assumed several crystal structure

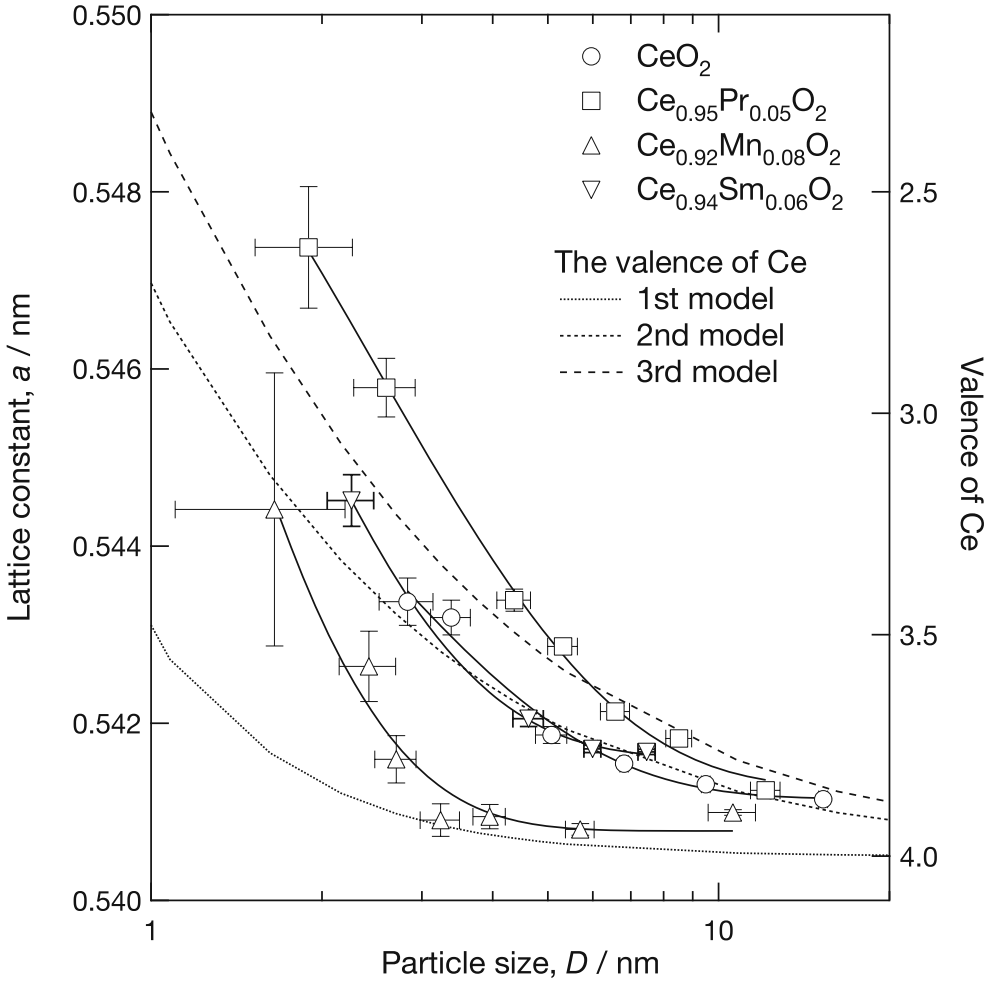

Fig. 4 Particle size dependence of lattice constant of pure ceria and Pr-, Mn- and Sm-doped ceria nanoparticles determined from XRD method. Dashed lines indicates the valence of Ce cations calculated by Tsunekawa et al. [22]

models. The first model is no vacancy model, that is, all of four oxygen atoms on surface hold the valence of -1 (peroxide). The second one is that the number of oxygen atoms on the surface is half (two oxygen atoms and two vacancies) and the valence of the atoms is also −1. The third one is that the arrangement is same as that for the second model but the valence of the atoms is −0.5 (superoxide) [22]. From electrostatic charge neutrality, then, Ce^{3+} needs to be formed on Ce^{4+} sites as a result of the reduction process. As shown in Fig. 4, the lattice expansion becomes significant, in other words, the amount of Ce^{3+} increases in the order of first, second and third models. Pure and Sm-doped ceria nanoparticles showed a good agreement with the second model. On the other hand, Pr- and Mn-doped ceria nanoparticles showed an agreement with 3rd and 1st models, respectively. This difference may be explained by the difference in a cation size of the dopants.

3.2 Electrical conductivity under high pressure

The electrical conductivity measurements under high pressure were conducted for Sm-doped ceria. Prior to the measurement of Sm-doped ceria nanoparticles, a bulk sample of 5 mol% Sm-doped ceria, which was sintered at 1500 °C for 20 h, with a relative density of approximately 93% and a grain size of approximately 2 to 5 μm was evaluated as a reference. Figure 5(a) shows the Cole-Cole plots of the bulk sample of 5 mol% Sm-doped ceria at 325 °C under 1 bar and 6 GPa. The presence of straight spikes at lower frequencies suggests that oxide-ions are major carriers. Based on an equivalent circuit analysis, the apparent semicircles can be reproduced by using a capacitance value on the order of 10^{-9} F. In addition, a small semicircle, which is unfortunately invisible in Fig. 5(a), was clearly observed for higher frequencies. From these observations, the apparent semicircles were found to correspond to a

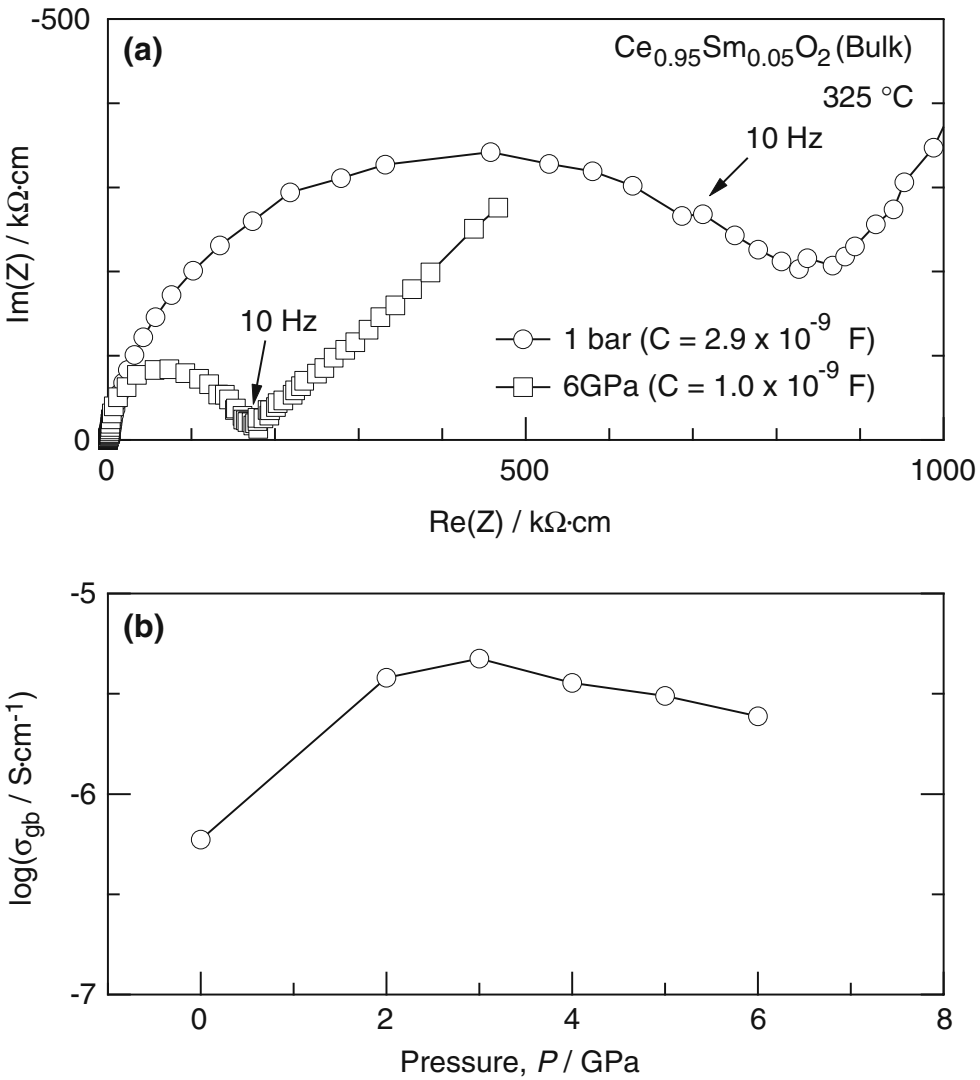

Fig. 5 (**a**) Cole-Cole plots of 5 mol%Sm-doped ceria prepared by the Pechini method under 1 bar and 6 GPa at 325 °C; (**b**) the electrical conductivity of grain boundary as a function of pressure

relaxation process for grain boundary. It should be then noted that the grain boundary conductivity increase by a factor of four under high pressure. The electrical conductivity of grain boundary (σ_{gb}) for the 5 mol% Sm-doped ceria at 325 °C is plotted as a function of pressure in Fig. 5(b). The electrical conductivity shows a shallow maximum at around 3 GPa, and slightly decrease with increasing pressure. The later decrease may be attributed to the effect of activation volume. Because of this activation volume effect, the electrical conductivity of grains also slightly decreased with increasing pressure.

Figure 6 shows the electrical conductivity of the 5 mol% Sm-doped ceria as a function of temperature. The enhancement of σ_{gb} can be clearly seen. In addition, it should be noticed that the enhancement is basically due to increase in a pre-exponential term, indicating the enhancement of carrier concentration under high pressure. This result encourages the electrical conductivity measurement for the nanoparticles under high pressure.

The electrical conductivity measurement for Sm-doped ceria nanoparticles was then performed under high pressure. The Sm-doped ceria nanoparticles annealed at 400 °C for 10 h, having a grain size of approximately 6 nm, was subjected to the measurement. The annealing at 400 °C was performed in order to remove water which may be incorporated into the nanoparticles during preparation and/or adsorbed on their surface. The dehydration process was monitored by a thermogravimetric technique. Figure 7 shows SEM photographs of the Sm-doped ceria nanoparticles (a) before and (b) after the electrical conductivity measurement at 300 °C under 6 GPa. As can be seen, the sample was fully densified even at 300 °C; the relative density was found to be reaching to 93%. The grain size

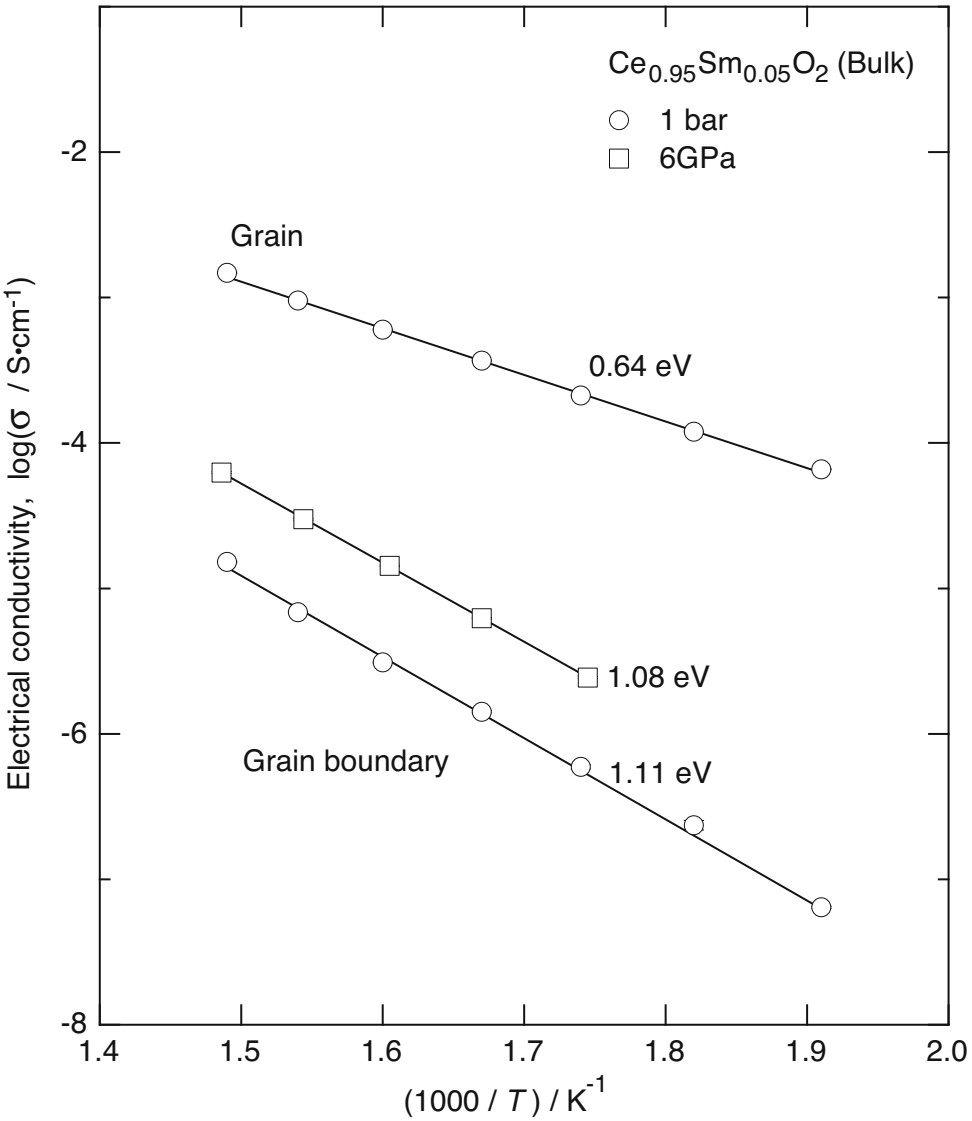

Fig. 6 Arrhenius-type plots of grain and grain-boundary electrical conductivity of 5 mol% Sm-doped ceria prepared by the Pechini method

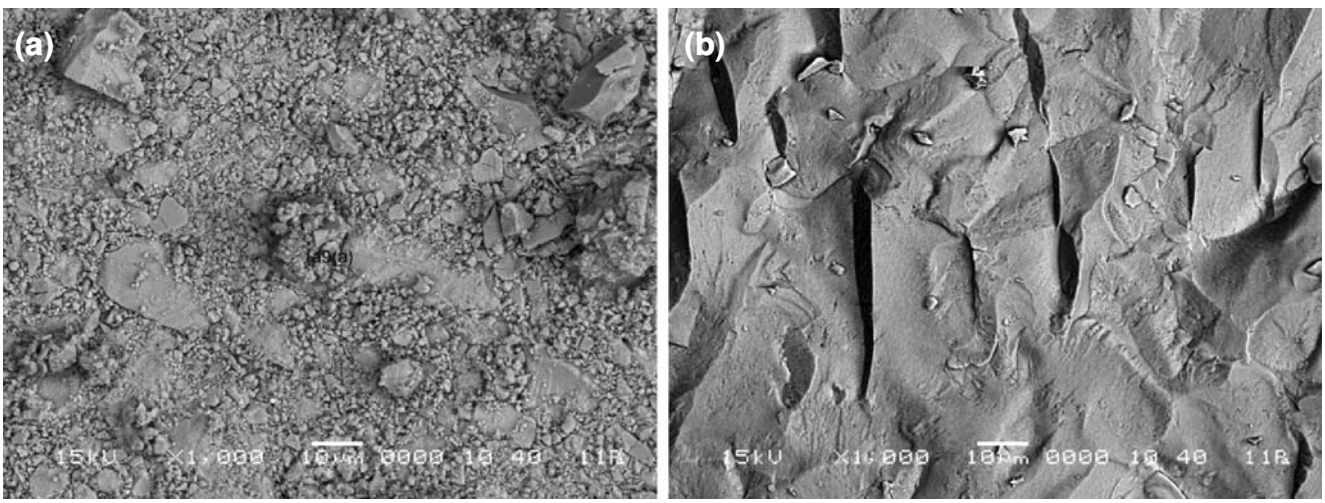

Fig. 7 SEM images of 6 mol% Sm-doped ceria nanoparticles annealed at 400 °C for 10 h; (**a**) before and (**b**) after high pressure measurement at 300 °C under 6 GPa

was confirmed by means of XRD after the measurement; the grain size was found to be slightly increased to 7.4 nm. The electrical conductivity of the Sm-doped ceria nanoparticles was calculated by using the sample dimensions after measurements.

Figure 8 shows the electrical conductivity of the 6 mol% Sm-doped ceria nanoparticles (annealed at 400 °C; grain size, D = 6.0 nm) as a function of temperature. In the figure, the data in Fig. 6 is also plotted for comparison. As can be seen, the sample of 6 mol% Sm-doped ceria nanoparticles (filled squares) shows higher electrical conductivity than that for the sample with μm-scale grains; The electrical conductivity is approximately 3×10^{-3} S/cm at 300 °C under 6 GPa. The enhanced electrical conductivity, however, tends to be constant as temperature increases, and then finally decreases during cooling process. It should be noted that the temperature at which the electrical conductivity tends to be constant shows a good agreement with the annealing temperature of 400 °C (1000/T in K ≈ 1.48). In the case that temperature was decreased without exceeding the annealing temperature, the electrical conductivity decreased in accordance with an activation energy of approximately 0.38 eV. This implies that nano-size grains and/or grain boundaries may be responsible for the enhancement of electrical conductivity. In addition, the Cole-Cole plot of the 6 mol% Sm-doped ceria nanoparticles at 274 °C (see an inset) showing a spike at lower frequency and capacitance on the order of 10^{-9} F suggests that the electrical conductivity enhancement may originate from ionic conduction.

To clarify the pressure effect, the electrical conductivity measurement was performed for the same

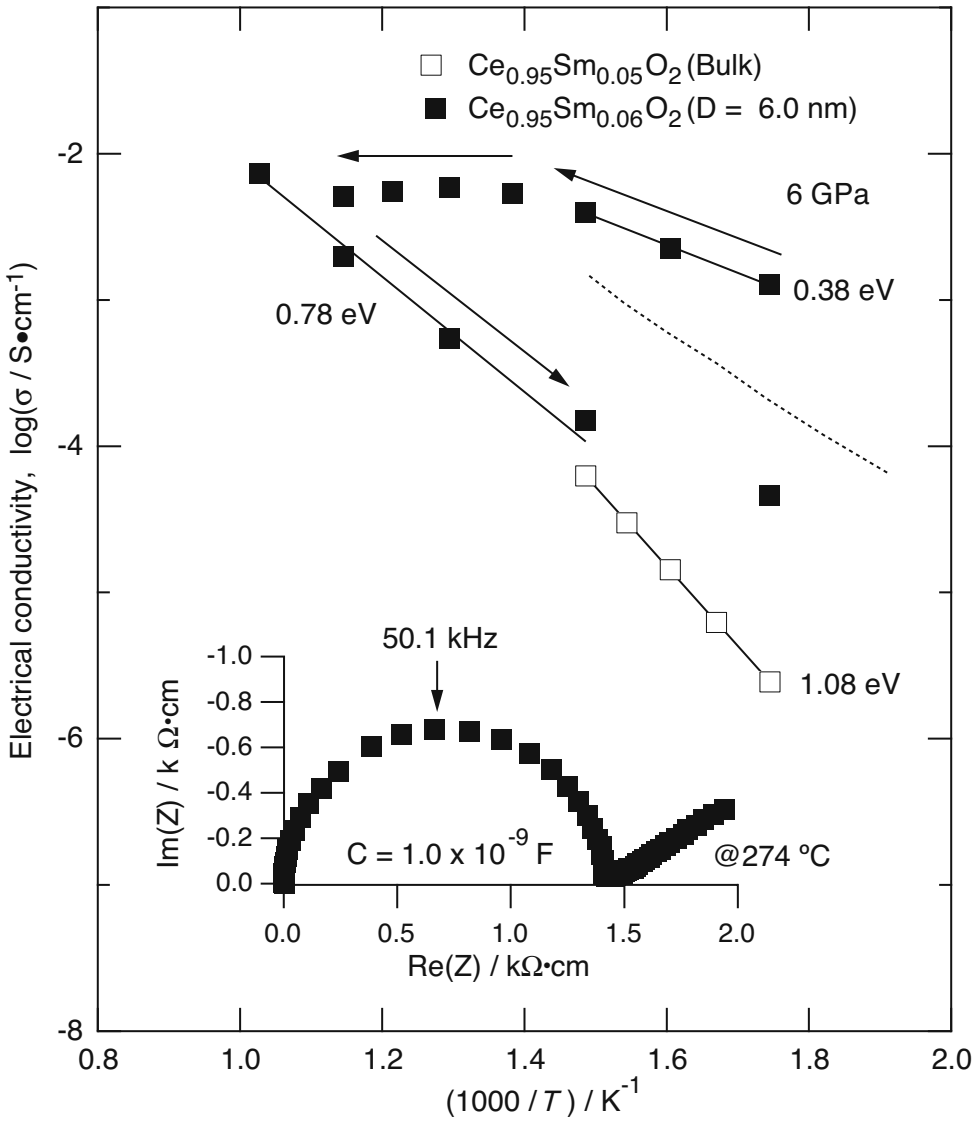

Fig. 8 Arrhenius-type plots of electrical conductivity of 6 mol%Sm-doped ceria nanoparticles under 6 GPa. The data in Fig. 6 is also plotted. An *inset* is the Cole-Cole plot of 6 mol%Sm-doped ceria nanoparticles at 274 °C under 6 GPa

sample under ambient pressure after pressure release. At room temperature, an electrical conductivity of 1.6×10^{-7} S/cm was observed; however, the electrical conductivity decreased with increasing temperature under ambient pressure. At 300 °C, an electrical conductivity on the order of 10^{-8} S/cm was obtained. After cooling, the same sample was placed into the high pressure apparatus again to check the reversibility of electrical conductivity with respect to pressure. As a result, this sample was found to exhibit an electrical conductivity of 4.7×10^{-5} S/cm at 300 °C under 6 GPa; this value is somewhere between the electrical conductivity of the initial measurement under high pressure (3×10^{-3} S/cm) and that of bulk sample (2.4×10^{-6} S/cm), suggesting that reversible and irreversible effects are mixed. This behavior with respect to pressure release and re-application might be attributed to the possibility of proton conduction due to adsorbed and/or structural water. In fact, an activation energy of 0.38 eV is quite low as an oxide-ion conductor [23]; on the other hand, an activation energy for surface proton conduction can be as low as 0.15 eV [24, 25]. In addition, proton conduction in nano-YSZ has been reported [26]. From these observations, it can be said that the enhancement of ion conductivity can be observed for ceria nanoparticles by using high pressure on the order of giga pascal, even though further analysis, especially the determination of ionic carrier with respect to the amount of adsorbed and/or structural water, is required.

4 Conclusions

The electrical conductivity of ceria nanoparticles under high pressure was investigated in this study. Pure and acceptor-doped ceria nanoparticles with a grain size of approximately 2 nm were prepared by mixing hexamethylenetramine and metal nitrate solutions. The size of ceria nanoparticles was controlled to be 2 to 15 nm by varying heat-treatment conditions. By applying a pressure of 6 GPa at 300 °C, the green compact of 6 mol% Sm-doped ceria nanoparticles was densified; a relative density of 93% was achieved. The sample showed an electrical conductivity of 3×10^{-3} S/cm at 300 °C under 6 GPa. The enhancement of electrical conductivity under high pressure seems to be related to ionic conduction in the vicinity of grain boundaries.

Acknowledgements This work has been supported in part by Industrial Technology Research Grant Program from New Energy and Industrial Technology Development Organization (NEDO) of Japan, and Program for Improvement of Research Environment for Young Researchers from Special Coordination Funds for Promoting Science and Technology (SCF) commissioned by the Ministry of Education, Culture, Sports, Science and Technology (MEXT) of Japan.

References

1. M. Nauer, C. Ftikos, B.C.H. Steele, J. Eur. Ceram. Soc. **14**, 493 (1994)
2. C. Ftikos, S. Carter, B.C.H. Steele, J. Eur. Ceram. Soc. **12**, 267 (1993)
3. Y. Takasu, T. Sugino, Y. Matsuda, J. Appl. Electrochem. **14**, 79 (1984)
4. H. Takamura, K. Okumura, Y. Koshino, A. Kamegawa, M. Okada, J. Electroceram. **13**, 613 (2003)
5. Y.M. Chiang, E.B. Lavik, I. Kosacki, H.L. Tuller, Appl. Phys. Lett. **69**, 185 (1996)
6. Y.M. Chiang, E.B. Lavik, I. Kosacki, H.L. Tuller, J. Electroceram. **1**, 7 (1997)
7. J. Maier, Prog. Solid State Chem. **23**, 171 (1995)
8. H.L. Tuller, Solid State Ionics **131**, 143 (2000)
9. A. Tschöpe, E. Sommer, R. Birringer, Solid State Ionics **139**, 255 (2001)
10. A. Tschöpe, Solid State Ionics **139**, 267 (2001)
11. A. Tschöpe, S. Kilassonia, B. Zapp, R. Birringer, Solid State Ionics **149**, 261 (2002)
12. A. Tschöpe, S. Kilassonia, R. Birringer, Solid State Ionics **173**, 57 (2004)
13. P. Knauth, Solid State Ionics **177**, 2495 (2006)
14. N. Blazevic, D. Kolbah, Synthesis 161 (1979)
15. J.M. Dreyfors, S.B. Jones, Y. Sayed, Am. Ind. Hyg. Assoc. J. **50**, 579 (1989)
16. H.P. Klug, L.E. Alexander, *X-Ray Diffraction Procedures* (Wiley, New York, 1974), pp. 634
17. J. He, J. Ye, E.J. Laverniaz, D. Matejczyk, C. Bampton, J.M. Schoenung, J. Mater. Sci. **39**, 6957 (2004)
18. Z. Zhang, F. Zhou, E.J. Lavernia, Metall. Mater. Trans. A **34**, 1349 (2003)
19. H. Takamura, H. Kakuta, A. Kamegawa, M. Okada, H.L. Tuller, Mater. Res. Soc. Symp. Proc. **835**, K2.10.1 (2005)
20. P. Chen, I. Chen, J. Am. Ceram. Soc. **76**, 1577 (1993)
21. J. Kobayashi, H. Takamura, A. Kamegawa, M. Okada, Mater. Res. Soc. Symp. Proc. **885E**, 0885-A03-08 (2006)
22. S. Tsunekawa, R. Sahara, Y. Kawazoe, K. Ishikawa, Appl. Surf. Sci. **152**, 53 (1999)
23. S. Kim, J. Maier, J. Electrochem. Soc. **149**, J73 (2002)
24. Y.M. Li, M. Hibino, M. Miyayania, T. Kudo, Solid State Ionics **134**, 271 (2000)
25. K. Hinokuma, M. Ata, Chem. Phys. Lett. **341**, 442 (2001)
26. U. Anselmi-Tamburini, F. Maglia, G. Chiodelli, P. Riello, S. Bucella, Z.A. Munira, Appl. Phys. Lett. **89**, 163116 (2006)